

Highlights

Spatiotemporal stability of synchronized coupled map lattice states

Domenico Lippolis

- A spatiotemporal orbit Jacobian is computed for coupled map lattices in the first Brillouin zone.
- The linear stability of synchronized states under periodic and aperiodic perturbations is studied.
- Short periodic orbits exhibit a nontrivial dependence of the stability exponent on the lattice coupling.

Spatiotemporal stability of synchronized coupled map lattice states

Domenico Lippolis

Department of Physics, Tokyo Metropolitan University, Hachioji, 192-0397, Japan

ARTICLE INFO

Keywords:

Spatiotemporal chaos
Synchronized states
Orbit Jacobian
Bravais stability

ABSTRACT

In the realm of spatiotemporal chaos, unstable periodic orbits play a major role in understanding the dynamics. Their stability changes and bifurcations in general are thus of central interest. Here, coupled map lattice discretizations of nonlinear partial differential equations, exhibiting a variety of behaviors depending on the coupling strength, are considered. In particular, the linear stability analysis of synchronized states is performed by evaluating the Bravais lattice orbit Jacobian in its reciprocal space first Brillouin zone, with space and time treated on equal grounds. The eigenvalues of the orbit Jacobian operator, computed as functions of the coupling strength, tell us about the stability of the periodic orbit under a perturbation of a certain time- and space frequency. Moreover, the stability under aperiodic, that is, incoherent perturbations, is revealed by integrating the sum of the stability exponents over all space-time frequencies.

1. Introduction

Consider a scalar field $\varphi(\vec{x}, t)$ described by a reaction-diffusion PDE

$$\frac{\partial}{\partial t} \varphi = D \cdot \Delta \varphi + V'(\varphi), \quad (1)$$

where the linear part is the heat equation, D is a diffusion constant or a diffusion tensor, and V is a potential. In one space dimension the Laplacian is $\Delta = \partial^2 / \partial x^2$. Ginzburg-Landau type equations and nonlinear Schrödinger equations are examples of such systems. Nonlinear PDEs of this kind may showcase a wide variety of dynamical behaviors, from integrability, to Turing instabilities, to full-fledged spatiotemporal chaos, and may serve as a model to describe phenomena of virtually every energy scale.

Space-time discretizations of reaction-diffusion PDEs can make integration more practical, and the analysis more insightful [18]. Out of the many realizations in the literature, Kaneko's 'diffusive coupled map lattice' spacetime discretization of (1) is considered here [24, 25]. One makes the discretized coordinates an integer hypercubic lattice \mathbb{Z}^d by scaling the lattice constants Δx , Δt to unit spacing, and by rescaling $\varphi(x, t)$ into a dimensionless field $\phi_{n,t}$. The resulting discretized defining equation (1) is

$$\phi_{n,t+1} - \phi_{n,t} = \frac{a}{2} (\phi_{n+1,t} - 2\phi_{n,t} + \phi_{n-1,t}) + (1-a)(F(\phi_{n,t}) - \phi_{n,t}). \quad (2)$$

Here $(n, t) \in \mathbb{Z}^2$ are integer square lattice spacetime positions, a is the dimensionless diffusion constant $a = 2D \Delta t / (\Delta x)^2$, the Laplacian couples neighboring lattice site fields with strength a , and F is forward-in-time map at each site nt , related to the potential in (1) by

$$V'(\phi_{n,t}) = (1-a)(F(\phi_{n,t}) - \phi_{n,t}). \quad (3)$$

As the correspondence between Eqs. (1) and (2) shows, coupled map lattices lend themselves to approximating less tractable continuous systems, such as those describing turbulence [6, 3, 10]. They have been studied theoretically [9, 20, 11], phenomenologically as paradigms of pattern formation [27], as well as experimentally [21]. Farther-reaching applications include neural networks [35], cryptography [41], and most recently, reservoir computing [31].

In his chaotic quantization of field theories [4], C. Beck introduces the coupled map lattice (2) with the map $F(\phi)$ in Eq. (3) given by the Chebyshev polynomials

$$T_N(\phi) = \cos(N \arccos \phi), \quad |\phi| \leq 1, \quad (4)$$

 lippolis@tmu.ac.jp (D. Lippolis)

 <https://cns.gatech.edu/~domenico/> (D. Lippolis)

ORCID(s): 0000-0002-2817-0859 (D. Lippolis)

in order to replace Gaussian noise by deterministic chaos in the Parisi-Wu stochastic quantization [36]. Chebyshev maps, as constituents of the many-body chains (2) evolving in discrete time, are smoothly conjugated to Bernoulli shifts and thus strongly chaotic. In spite of that, stable synchronized states at small couplings have been discovered (Dettmann [16]) for this model.

The emergence of coherent structures [8] and the study of instability fields [22, 32, 37, 23, 1] in coupled map lattices have been issues of great relevance for decades, due to the rich dynamical landscape offered by these models, as well as the effectiveness of such tools as the properly defined Lyapunov exponents and Lyapunov vectors.

Recently, the study of the stability of spatiotemporal recurrent patterns has found application in chaotic lattice field theories [33, 15], whose partition functions are written as sums over periodic orbits in spacetime geometries. The weights of the periodic orbits depend on their instabilities, evaluated by linearizing the dynamics on a lattice, where spatial and temporal directions are treated on equal footing, and evaluated on the reciprocal lattice, by means of Bloch's theorem.

The operation of Fourier-transforming to a wavenumber-frequency space (in both real space and time) emphasizes an aspect of dynamics, which is at the center of the present study: linear stability analysis as we know it deals with the response of a *periodic* orbit to *periodic* perturbations, best characterized in reciprocal space by their frequencies. Yet, perturbations are in general aperiodic, or incoherent, and may be obtained from superpositions of all frequencies, for a thorough stability analysis.

Here, the stability properties are investigated in a special family of periodic orbits, the synchronized states [38, 40] of the evolving chain (2). In particular, the goal of the analysis is to describe the behavior of the stability exponents of the synchronized states as a function of the lattice coupling strength, as well as to demonstrate that short periodic orbits become stable [16] under coherent and incoherent perturbations, for large enough couplings.

The article is organized as follows: in section 2, the differences are explained between the time-forward and the spatiotemporal approaches to linear stability analysis; in section 3, the spatiotemporal orbit Jacobian operator in reciprocal space is introduced; the spatiotemporal linear stability analysis is then performed on the synchronized states of the coupled Chebyshev map lattices in section 4, and in particular on steady states (section 4.1), as well as on period-2 orbits (section 4.2). Conclusions are drawn in section 5.

2. Forward-in-time- versus spatiotemporal orbit Jacobian operator

Linear stability is typically evaluated through the familiar forward-in-time Jacobian, obtained as follows. First, rewrite the discretized defining equation (2) as a forward-in-time map:

$$\phi_{n,t+1} = (1-a)T_N(\phi_{n,t}) + \frac{a}{2}(\phi_{n-1,t} + \phi_{n+1,t}). \quad (5)$$

Here, the N th Chebyshev polynomial $T_N(\phi)$ defined in (4) replaces the general $F(\phi)$ in Eq. (2). The forward-in-time evolution of perturbations is given by

$$\delta\Phi_{t+1} = J_t \delta\Phi_t, \quad [J_t]_{mn} = \frac{\partial \phi_{m,t+1}}{\partial \phi_{n,t}}, \quad (6)$$

where $\Phi_t = (\phi_{0,t}, \dots, \phi_{L-1,t})^T$, and the $L \times L$ temporal Jacobian is

$$J_t = \begin{pmatrix} (1-a)T'_N(\phi_0) & \frac{a}{2} & 0 & 0 & \dots & \frac{a}{2} \\ \frac{a}{2} & (1-a)T'_N(\phi_1) & \frac{a}{2} & 0 & \dots & 0 \\ 0 & \frac{a}{2} & (1-a)T'_N(\phi_2) & \frac{a}{2} & \dots & 0 \\ \dots & \dots & \dots & \dots & \dots & \dots \\ \frac{a}{2} & 0 & 0 & \dots & \frac{a}{2} & (1-a)T'_N(\phi_{L-1}) \end{pmatrix}. \quad (7)$$

In this temporal picture, the full stability matrix of an orbit $\{\Phi_0, \Phi_1, \dots, \Phi_{\tau-1}\}$ is the product of the J_t 's computed at each point,

$$J = J_{\tau-1} J_{\tau-2} \cdots J_0. \quad (8)$$

The stability of J then depends on its eigenvalues.

On the other hand, the orbit Jacobian operator [7] describes the linearized evolution on the full spatiotemporal lattice, and it is obtained by differentiating Eq. (2):

$$\mathcal{J}_{n't',n} = (\delta_{t',t+1} - \delta_{t',t})\delta_{n',n} - \frac{a}{2}(\delta_{n',n-1} - 2\delta_{n',n} + \delta_{n',n+1})\delta_{t',t} - V''(\phi_{n,t})\delta_{n',n}\delta_{t',t}, \quad (9)$$

where $V''(\phi)$ is given by Eq. (3) with $F = T_N(\phi)$. If we consider a spatiotemporal cell of size $[L \times \tau]$, the orbit Jacobian matrix \mathcal{J} is a $L\tau \times L\tau$ matrix, much larger in general than the temporal Jacobian J . If the orbit $\{\Phi_0, \Phi_1, \dots, \Phi_{\tau-1}\}$ is periodic, the determinants of the temporal and orbit Jacobian operators are related by Hill's formula [33]

$$|\det \mathcal{J}| = |\det (1 - J)|. \quad (10)$$

For the sake of clarity, let us compare these two notions of stability in the simple example of a single-site spatiotemporal lattice.

2.1. One spatial lattice site Jacobian

Consider a one-dimensional lattice, infinitely extended in time, but with only one site in the spatial dimension. In this case, the orbit Jacobian matrix (9) reduces to

$$\mathcal{J}_{t',t} = \delta_{t',t+1} - \delta_{t',t} - V''(\phi_t)\delta_{t',t}. \quad (11)$$

For a periodic orbit of temporal period τ , Eq. (11) reads, in matrix form,

$$\mathcal{J} = \begin{pmatrix} -1 - V''_0 & 1 & 0 & 0 & \dots & 0 \\ 0 & -1 - V''_1 & 1 & 0 & \dots & 0 \\ 0 & 0 & -1 - V''_2 & 1 & \dots & 0 \\ \dots & \dots & \dots & \dots & \dots & \dots \\ 1 & 0 & 0 & 0 & \dots & -1 - V''_{\tau-1} \end{pmatrix}. \quad (12)$$

The determinant of \mathcal{J} can be expanded with respect to the first column, and so written as a sum of two circulants:

$$\det \mathcal{J} = (-1 - V''_0)K_{\tau-1} + (-1)^{\tau-1}K_{1,\tau-1}, \quad (13)$$

with

$$K_{\tau-1} = \begin{vmatrix} -1 - V''_1 & 1 & 0 & 0 & \dots & 0 \\ 0 & -1 - V''_2 & 1 & 0 & \dots & 0 \\ 0 & 0 & -1 - V''_3 & 1 & \dots & 0 \\ \dots & \dots & \dots & \dots & \dots & \dots \\ 0 & 0 & 0 & 0 & \dots & -1 - V''_{\tau-1} \end{vmatrix}, \quad (14)$$

and

$$K_{1,\tau-1} = \begin{vmatrix} 1 & 0 & 0 & 0 & \dots & 0 \\ -1 - V''_1 & 1 & 0 & \dots & 0 & \\ 0 & -1 - V''_2 & 1 & \dots & 0 & \\ \dots & \dots & \dots & \dots & \dots & \dots \\ 0 & 0 & 0 & \dots & -1 - V''_{\tau-2} & 1 \end{vmatrix}. \quad (15)$$

The previous are both determinants of triangular matrices, and thus Eq. (13) is finally

$$\det \mathcal{J} = \prod_{i=0}^{\tau-1} (-1 - V''_i) + (-1)^{\tau-1} = (-1)^{\tau-1} + (-1)^\tau \prod_{i=0}^{\tau-1} [a + (1-a)T'_N(\phi_i)]. \quad (16)$$

In order to compare Eq. (16) with the result $|\det (1 - J)|$ from the temporal calculation, recall the map (5) for a one-site lattice

$$\phi_{t+1} = (1-a)T_N(\phi_t) + a\phi_t. \quad (17)$$

The temporal Jacobian is one-dimensional and simply given by the product of the derivatives of the above expression, resulting in the determinant

$$\det(1 - J) = 1 - \prod_{t=0}^{\tau-1} [a + (1 - a)T'_N(\phi_t)], \quad (18)$$

which is the same as (16) in absolute value.

3. Orbit Jacobian operator in reciprocal space

The Jacobian determinant is associated to the stability of a periodic orbit of period τ to a perturbation of the same period, or of a multiple of it (repeat). Equivalently, one can switch to a reciprocal lattice where periods are replaced by frequencies, just like it is usually done in condensed matter physics with Bravais lattices. The advantage of using reciprocal space is at least twofold: first, this representation accounts for cyclic translations [15] of the same orbit, and therefore automatically operates a partial symmetry reduction of the periodic orbits on the lattice; secondly, as it will be explained below for synchronized states, the stability exponents of each orbit can be summed over perturbations of all frequencies, obtaining the stability under incoherent, that is aperiodic, perturbations.

The first goal of the stability analysis in the reciprocal lattice is to obtain the eigenvalues of the Jacobian for a given perturbation frequency. In the temporal representation, this is most easily achieved by searching for complex eigenvalues of the cyclic matrix J [Eq. (8)] of the form [16]

$$\Lambda_k = \sum_{n=0}^{L-1} b_n e^{ink}, \quad (19)$$

with $k = 2\pi n/L$, in a space of eigenvectors of the form $v_k = (1, e^{ik}, e^{2ik}, \dots, e^{-ik})^\top$. Applying $Jv_k = \Lambda_k v_k$ yields

$$\Lambda_k = \prod_{t=0}^{\tau-1} [(1 - a)T'_N(\phi_t) + a \cos k]. \quad (20)$$

On the other hand, in the spatiotemporal picture, the eigenvalues and the determinant of the orbit Jacobian matrix in reciprocal space are obtained by first taking the discrete Fourier transform $\tilde{J}_{m,m'}$ [with $m = (m_1, m_2)$] of the matrix element $J_{n't',n}$ [Eq. (9)]:

$$\begin{aligned} \tilde{J}_{m,m'} &= \sum_{n't't} e^{i(k_1 t - k'_1 t') + i(k_2 n - k'_2 n')} (\delta_{t',t+1} - \delta_{t',t}) \delta_{n',n} - \sum_{n't't} e^{i(k_1 t - k'_1 t') + i(k_2 n - k'_2 n')} V''(\phi_{nt}) \delta_{n',n} \delta_{t',t} \\ &- \frac{a}{2} \sum_{n't't} e^{i(k_1 t - k'_1 t') + i(k_2 n - k'_2 n')} (\delta_{n',n-1} - 2\delta_{n',n} + \delta_{n',n+1}) \delta_{t',t} = \\ &= \sum_{n,t} e^{i(k_1 - k'_1)t + i(k_2 - k'_2)n} (e^{-ik'_1} - 1) - \sum_{n,t} e^{i(k_1 - k'_1)t + i(k_2 - k'_2)n} V''(\phi_{n,t}) \\ &- \frac{a}{2} \sum_{n,t} e^{i(k_1 - k'_1)t + i(k_2 - k'_2)n} (e^{ik'_2} - 2 + e^{-ik'_2}) \end{aligned} \quad (21)$$

$$= (e^{-ik'_1} - 1) \delta_{m',m} - \tilde{V}''(\phi) - a(\cos k'_2 - 1) \delta_{m',m}, \quad (22)$$

where the term $\tilde{V}''(\phi) = \sum_{n,t} e^{i(k_1 - k'_1)t + i(k_2 - k'_2)n} V''(\phi_{n,t})$ produces the non-diagonal entries in the reciprocal Jacobian.

Here $k_1 = \frac{2m_1\pi}{\tau}$, $k_2 = \frac{2m_2\pi}{L}$, $m = (m_1, m_2)$, with $m_1 = 0, \dots, \tau - 1$, and $m_2 = 0, \dots, L - 1$, for a rectangular primitive cell $[L \times \tau]$ of spatial period L and temporal period τ . Then one computes the spectrum of the orbit Jacobian operator \tilde{J} , which is now shown in the special case of synchronized states, and compared to the temporal result (20).

4. Spatiotemporal stability of synchronized states

Synchronized states are solutions in which $\phi_{n,t} = \phi_t$ is independent of the spatial position n , so are given by a one-dimensional map. They are the simplest bridge from 1-dimensional systems to their 2-dimensional transverse

modes, with continuous k stability. In chaotic field theory, the focus is on *unstable* periodic states. Among those, short temporal period solutions in particular are closely related to the unstable ones.

Regarding our model (2), it was established in Ref. [16] that what makes synchronized states still quite different from one-dimensional temporal lattice systems is their spacetime stability. It was found earlier [2, 19] for generic coupled map lattices, that the linear stability properties of the single-site periodic orbits carry over to the corresponding synchronized states (therein called homogenous solutions) only for temporal period $\tau = 1$, that is what we call fixed points or steady states. For cycles of longer periods, the stability of the synchronized states may in general differ from that of the 1-dimensional system.

The linear stability properties of the full coupled map lattice are slightly different from that of the synchronized map, so that although stability occurs in the region of synchronized superstable orbits, the superstable orbit may not be linearly stable in the extended system. The difference between stability in the synchronized map and the extended system is that the full coupled map lattice has an infinite number of degrees of freedom, leading to a richer spectrum of possible instabilities. Linear stability follows if all multipliers are contracting, for all L discrete eigenmodes.

In the next sections, the linear stability of time period-1 (steady states) and period-2 synchronized states is investigated of the coupled map (2), to periodic perturbations of all frequencies, or to aperiodic (incoherent) perturbations.

4.1. Steady states

Let us begin from the steady state, where the field has the same value across the lattice, and the term of self-interaction potential in the Jacobian (9) is constant:

$$V''(\phi_{n,t}) = V''(\phi_t) = (1 - a)(T'_N(\phi_t) - 1). \quad (23)$$

The synchronized steady state solves fixed-point condition for the map (5) with $\phi_{n,t} = \phi_t$:

$$\phi_t = (1 - a)T_N(\phi_t) + \frac{a}{2}(\phi_t + \phi_t). \quad (24)$$

For the Chebyshev $T_2(\phi) = 2\phi^2 - 1$ model, there are two fixed points, that is $\phi_0 = -1/2$ and $\phi_1 = 1$. Let us denote either fixed point with ϕ_p in the following analysis. At each steady state, the reciprocal orbit Jacobian matrix (22) is diagonal, since

$$\sum_{n,t} e^{i(k_1 - k'_1)t + i(k_2 - k'_2)n} V''(\phi_{n,t}) = V''(\phi_p) \sum_{n,t} e^{i(k_1 - k'_1)t + i(k_2 - k'_2)n} = (1 - a)(T'_N(\phi_p) - 1) \delta_{m',m}, \quad (25)$$

and, overall,

$$\tilde{\mathcal{J}}_{m,m'} = [e^{-ik_1} - (1 - a)T'_N(\phi_p) - a \cos k_2] \delta_{m',m}. \quad (26)$$

Eq. (26) is also the expression for the eigenvalues of the orbit Jacobian matrix, that can now be compared with those [16] of the temporal Jacobian J in Eq. (20) with $\tau = 1$:

$$\Lambda_k = (1 - a)T'_N(\phi_p) + a \cos k. \quad (27)$$

If, in the spatiotemporal picture, we choose the simplest primitive cell [$L \times 1$] for this steady state, we have $\tau = 1$, $m_1 = 0$, and the phase $e^{-ik_1} = 1$. Then, identifying the k_2 of Eq. (26) with the k of Eq. (27), $|\tilde{\mathcal{J}}_{m,m}|$ is the same as $|1 - \Lambda_k|$ from the temporal Jacobian. Equation (26) reveals the stability of the time period-1 synchronized state Φ_p under perturbations of time frequency k_1 and space frequency k_2 : unstable if $|\Lambda_{k_2,k_1}| = |\tilde{\mathcal{J}}_{m,m}| > 1$, stable if $|\Lambda_{k_2,k_1}| < 1$, marginally stable if $|\Lambda_{k_2,k_1}| = 1$. Analogously, the expression (27) for the single, k -dependent eigenvalue, should be greater than unity in absolute value. That is equivalent to requiring that

$$T'_N(\phi_p) > \frac{1 - a \cos k}{1 - a}, \quad \text{or} \quad T'_N(\phi_p) < -\frac{1 + a \cos k}{1 - a}, \quad (28)$$

depending on whether $T'_N(\phi_p) > 0$ or $T'_N(\phi_p) < 0$. Fig. 1 tells us that, for small coupling a , all eigenvalues are unstable, and thus the steady state ϕ_p is unstable to perturbations of all space-frequencies. However, for large enough a

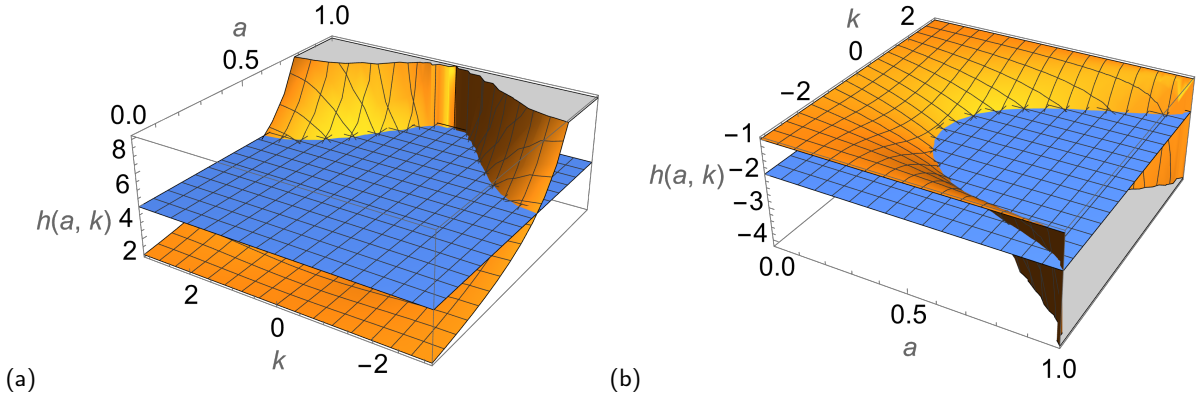


Figure 1: The range of a and k that makes Λ_k unstable is the region where the plane $z = T'_N(\phi_p)$ (in blue) is: (a) higher than the surface $h(a, k) = \frac{1-a \cos k}{1-a}$ (in orange) in the T_2 model with steady state $\phi_1 = 1$; (b) lower than the surface $h(a, k) = -\frac{1+a \cos k}{1-a}$ (in orange), T_2 model with steady state $\phi_0 = -1/2$.

the inequalities (28) no longer hold for all k 's, and so stable eigenvalues appear, meaning that the steady state is stable to perturbations of a certain frequency range $[-k^*, k^*]$. More and more eigenvalues become stable as a increases. In the limit $a \rightarrow 1$, the right-hand side of the inequalities (28) diverges, that is, in order to achieve mode instability in the limit of strongest coupling, it is required an infinite local stability multiplier.

The stability of the synchronized steady state under incoherent (aperiodic) perturbations is best determined by considering the spatiotemporal orbit Jacobian, and, in particular, by computing $\ln \det \mathcal{J}$. Equivalently, one can average the log of Eq. (26) over all frequencies [15], as

$$\lambda = \frac{1}{4\pi^2} \sum_{k_1, k_2} \Delta k_1 \Delta k_2 \ln \Lambda_{k_2, k_1}. \quad (29)$$

Recalling that $k_1 = \frac{2m_1\pi}{\tau}$, $k_2 = \frac{2m_2\pi}{L}$, the limit of the space and time periods of the primitive cell $L \rightarrow \infty$, $\tau \rightarrow \infty$ should be taken, with m_1, m_2 running from zero to infinity. The reason is that perturbations of a state can have the periodicity of the state itself, a different periodicity (or a different frequency in the Bravais lattice), or no periodicity at all [39], that is a superposition of incoherent frequencies. In the summation (29), $\Delta k_1 = \frac{2\pi}{T}$ and $\Delta k_2 = \frac{2\pi}{L}$. In the limit, the wavenumbers k are continuous, and conventionally restricted to the first Brillouin zone $\mathbb{B} = \{k_1 \in (-\pi/T, \pi/T]\} \cup \{k_2 \in (-\pi/L, \pi/L]\}$, since the Bravais lattice is periodic and the k -vectors exceeding \mathbb{B} do not carry any more information than their counterparts. Then, the Bravais stability exponent (29) is given as the integral

$$\lambda = \frac{1}{4\pi^2} \int_{-\pi}^{\pi} dk_2 \int_{-\pi}^{\pi} dk_1 \ln \Lambda_{k_1, k_2}. \quad (30)$$

In the specific case of the synchronized steady state of the Chebyshev lattice, the previous reads

$$\lambda = \frac{1}{4\pi^2} \int_{-\pi}^{\pi} dk_2 \int_{-\pi}^{\pi} dk_1 \ln [e^{-ik_1} - (1-a)T'_N(\phi_p) - a \cos k_2]. \quad (31)$$

The integral in dk_1 is of the form

$$I(a) = \int_{-\pi}^{\pi} dk_1 \ln [e^{-ik_1} + f(a, k_2)], \quad (32)$$

with $f(a, k_2) = -(1-a)T'_N(\phi_p) - a \cos k_2$. This can be evaluated by first differentiating with respect to a :

$$\frac{dI(a)}{da} = \int_{-\pi}^{\pi} dk_1 \frac{f'(a, k_2)}{e^{-ik_1} + f(a, k_2)} = \begin{cases} \frac{2\pi f'(a, k_2)}{f(a, k_2)}, & |f(a, k_2)| > 1 \\ 0, & |f(a, k_2)| < 1 \end{cases}, \quad (33)$$

Spatiotemporal stability of synchronized states

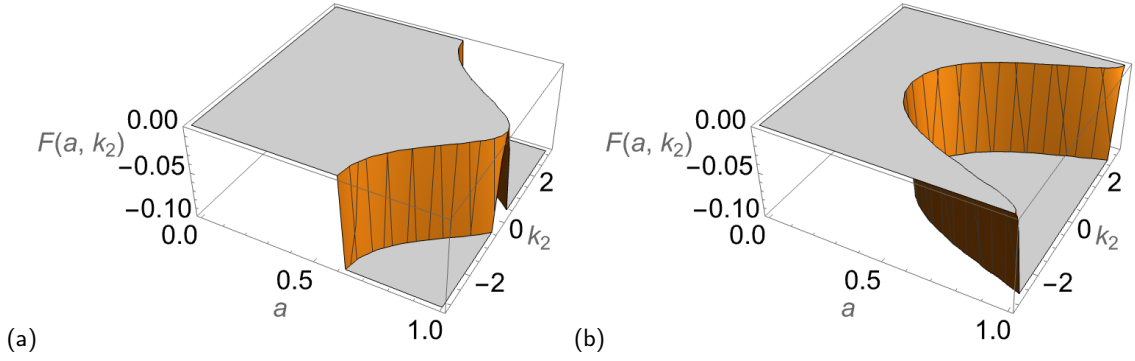


Figure 2: The range of a and k_2 that make $|f(a, k_2)| < 1$ is the interval where the function $F(a, k_2) = |f(a, k_2)| - 1$ is negative. (a) T_2 model and $\phi_1 = 1$. (b) T_2 model and $\phi_0 = -1/2$.

as a result of the residue theorem:

$$\frac{dI(a)}{da} = \oint_{\Gamma} \frac{dz}{iz} \frac{f'(a, k_2)}{z + f(a, k_2)},$$

(34)

There are two poles at $z_0 = 0$ and $z_1 = -f(a, k_2)$, and the latter is not enclosed by the contour Γ if $|f(a, k_2)| > 1$, equivalent to

$$a < \min \left[\frac{T'_N(\phi_p) - 1}{T'_N(\phi_p) - \cos k_2}, \frac{T'_N(\phi_p) + 1}{T'_N(\phi_p) - \cos k_2} \right],$$

(35)

which depends on the sign of $T'_N(\phi_p)$. If the previous inequality is verified, the pole z_1 lies outside Γ , and the integral is

$$\frac{dI(a)}{da} = 2\pi i \text{Res}(z_0) = \frac{2\pi f'(a, k_2)}{f(a, k_2)}.$$

(36)

If, instead, $|f(a, k_2)| < 1$, both poles contribute equal and opposite terms to the contour integral:

$$\frac{dI(a)}{da} = 2\pi i [\text{Res}(z_0) + \text{Res}(z_1)] = 2\pi \left(\frac{f'(a, k_2)}{f(a, k_2)} - \frac{f'(a, k_2)}{f(a, k_2)} \right) = 0.$$

(37)

In particular, the $k_2 = \pi$ that maximizes the denominator of the above expression yields an upper bound for a , such that (33) is nonzero. Beyond that, the integral does not vanish in a nontrivial range of k_2 , smaller than $[-\pi, \pi]$ (Fig. 2). Condition (35) is the same as (28) for the stability of the eigenvalues of the Jacobian vs. space frequency. Here it is retrieved independently, and expressed as an inequality for the lattice coupling strength a (cf. Fig. 1).

Let us now continue to evaluate the stability exponent (30). Suppose that (33) is nonzero, and so

$$I(a) = 2\pi \ln |f(a, k_2)| + c.$$

(38)

Because $I(0) = \ln |T'_N(\phi_p)| + c$ and that should just be the stability exponent of the one-dimensional fixed point, it must be $c = 0$. We are left with

$$\lambda = \frac{1}{2\pi} \int_{-\pi}^{\pi} dk_2 \ln |(1 - a)T'_N(\phi_p) + a \cos k_2|.$$

(39)

The integral is computed in Appendix A, and the result is

$$\lambda = \ln \frac{(1-a)|T'_N(\phi_p)| + \sqrt{(1-a)^2 T'^2_N(\phi_p) - a^2}}{2}, \quad (40)$$

with the condition

$$a < \frac{|T'_N(\phi_p)|}{1 + |T'_N(\phi_p)|}. \quad (41)$$

When $a = 0$ this again reduces to the one-dimensional stability exponent $\ln |T'_N(\phi_p)|$. Let us now compare the ranges of validity (35) and (41) for the above result. In the models considered here, $T'_2(\phi)$ is such that

$$\frac{T'_2(\phi_1) - 1}{T'_2(\phi_1) - \cos k_2} < \frac{T'_2(\phi_1)}{1 + T'_2(\phi_1)}, \quad \text{and} \quad \frac{T'_2(\phi_0) + 1}{T'_2(\phi_0) - \cos k_2} < \frac{T'_2(\phi_0)}{1 - T'_2(\phi_0)}, \quad (42)$$

so the Bravais stability exponent is equal to (40) when a is small enough to verify the inequality (35). For larger couplings, the integral (39) has limits of integration $\pm k_2^*$, where

$$k_2^* = \arccos \frac{1 - (1-a)T'_N(\phi_p)}{a}. \quad (43)$$

A primitive function does not seem to exist (discussion in Appendix A) for the integral in k_2 , so that the stability exponent

$$\lambda = \frac{1}{2\pi} \int_{-k_2^*}^{k_2^*} dk_2 \ln |(1-a)T'_N(\phi_p) + a \cos k_2| \quad (44)$$

is computed numerically, with the results portrayed in Figure 3.

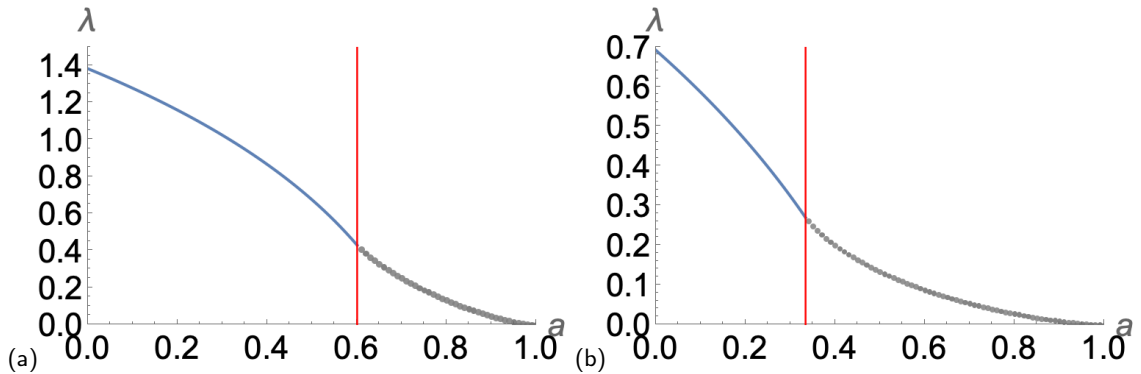


Figure 3: The stability exponent versus strength of coupling a (solid blue line). Beyond the red vertical line the condition $|f(a, k_2)| > 1$ no longer holds and thus the stability exponent is evaluated numerically (gray dots). (a) T_2 model for the steady state $\phi_1 = 1$ (b) T_2 model for the steady state $\phi_0 = -1/2$.

One can conclude that the steady states are always unstable under aperiodic perturbations, but their instability λ decreases with the lattice coupling. When the condition (35) [or, equivalently, (28), red vertical line in the figure] for the single eigenvalues Λ_{k_1, k_2} is no longer verified, some eigenvalues become stable, depending on the space frequency k_2 . Then, the Bravais stability exponent λ drops further, with the steady states tending towards stability ($\lambda \rightarrow 0$) as $a \rightarrow 1$. The observed behavior of the Bravais stability exponent reflects our qualitative understanding of the spatiotemporal lattice dynamics: in the anti-integrable regime $a = 0$ the dynamics is spatially decoupled, and instability is maximal since the individual T_N models on an interval yield strong chaos. On the other hand, spatial interplay grows complex as the coupling a is increased, so that these simplest synchronized states become less unstable, and eventually achieve maximum stiffness in the limit $a \rightarrow 1$.

4.2. Period-2 synchronized state

The next case is that of a temporal period-2 state, where, in the language of symbolic dynamics, the potential may take on two values, $V(\phi_t) = V_{01}$ or V_{10} , same for all n 's and at alternate times t . This periodic orbit is the solution to the system

$$\begin{aligned}\phi_{10} &= (1-a)T_N(\phi_{01}) + \frac{a}{2}(\phi_{01} + \phi_{01}) \\ \phi_{01} &= (1-a)T_N(\phi_{10}) + \frac{a}{2}(\phi_{10} + \phi_{10}).\end{aligned}\quad (45)$$

For the Chebyshev $T_2(\phi) = 2\phi^2 - 1$ model, that reads

$$\phi_{01/10} = \frac{-1-a \pm \sqrt{5-18a+9a^2}}{4-4a}.\quad (46)$$

Importantly, this synchronized state is real valued only in the interval $a \in [0, 1/3]$. The general entry (22) of $\tilde{\mathcal{J}}$ may thus be written as

$$\tilde{\mathcal{J}}_{m,m'} = \left[e^{-ik'_1} - 1 - a(\cos k'_2 - 1) \right] \delta_{m',m} - \frac{1}{2} \left[\sum_{t \text{ odd}} e^{i(k_1-k'_1)t} V''_{01} + \sum_{t \text{ even}} e^{i(k_1-k'_1)t} V''_{10} \right] \delta_{m'_2, m_2},\quad (47)$$

since the Fourier transforms over the spatial variable n can be performed by factoring out the sums over t , which are split into even and odd contributions.

Now consider the simplest primitive cell that can fit this state, that is $[L \times 2]$. In this case, $m_2 = 0, 1, \dots, L-1$, while $m_1 = 0, 1$. Then, the split Fourier transforms in Eq. (47) only count one term each, with phase

$$k_1 - k'_1 = \begin{cases} 0 & m_1 - m'_1 = 0 \\ \pm\pi & m_1 - m'_1 = \pm 1 \end{cases}.\quad (48)$$

Then the spatiotemporal orbit Jacobian operator in reciprocal space has diagonal entries

$$\tilde{\mathcal{J}}_{m,m} = e^{-ik_1} - 1 - a(\cos k_2 - 1) - \frac{1}{2} [V''_{01} + V''_{10}],\quad (49)$$

and off-diagonal entries

$$\tilde{\mathcal{J}}_{m_2, m_1, m_2(m_1 \pm 1)} = -\frac{1}{2} [V''_{01} - V''_{10}].\quad (50)$$

The eigenvalue Λ_{k_1, k_2} is evaluated via the relation $\tilde{\mathcal{J}} v_{k_1, k_2} = \Lambda_{k_1, k_2} v_{k_1, k_2}$, where v_{k_1, k_2} is a vector of $2L$ components (recall that $\tau = 2$), which we may take in the form $v_{k_1, k_2} = (a_+, a_-, a_+, a_-, \dots, a_+, a_-)^T$. Because the only non-zero entries of the orbit Jacobian matrix in reciprocal space are $\tilde{\mathcal{J}}_{m_2, m_1, m_2, m_1}$ and $\tilde{\mathcal{J}}_{m_2, m_1, m_2, m_1 \pm 1}$, every row of $\tilde{\mathcal{J}}$ has but two non-zero entries, and we end up with two coupled equations, one coming from the $(m_2, 0)$ -th row, and the other from the $(m_2, 1)$ -th row, so to speak (henceforth drop the index m_2 to simplify the notation, so as to keep track of m_1, m'_1 here below)

$$\tilde{\mathcal{J}}_{0,0} a_+ + \tilde{\mathcal{J}}_{0,1} a_- = \Lambda_{k_2, k_1} a_+ \quad (51)$$

$$\tilde{\mathcal{J}}_{1,1} a_- + \tilde{\mathcal{J}}_{1,0} a_+ = \Lambda_{k_2, k_1} a_-.\quad (52)$$

That brings a quadratic defining equation for Λ_{k_2, k_1} , whose solution reads

$$\Lambda_{k_2, k_1} = \frac{\tilde{\mathcal{J}}_{0,0} + \tilde{\mathcal{J}}_{1,1} \pm \sqrt{(\tilde{\mathcal{J}}_{0,0} - \tilde{\mathcal{J}}_{1,1})^2 + 4\tilde{\mathcal{J}}_{0,1}\tilde{\mathcal{J}}_{1,0}}}{2}.\quad (53)$$

As done for the steady state, let us now compute the Bravais stability of the period-2 synchronized state. Both Bloch bands computed in (53) contribute:

$$\lambda = \frac{1}{4\pi^2} \int_{-\pi}^{\pi} dk_2 \int_{-\pi/2}^{\pi/2} dk_1 (\ln |\Lambda_k^+| + \ln |\Lambda_k^-|).\quad (54)$$

It is noted that the domain of integration of k_1 is now reduced to $[-\pi/2, \pi/2]$, since the orbit Jacobian operator is invariant under translations of time-period $\tau = 2$. Each term in Eq. (54) brings an integral of the form

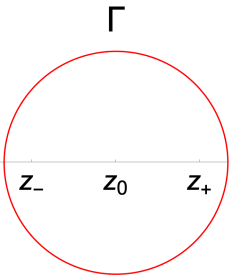
$$I(a) = \int_{-\pi/2}^{\pi/2} dk_1 \ln |g(a, k_2) \pm \sqrt{4e^{-2ik_1} + \Delta V''^2}|, \quad (55)$$

with

$$g(a, k_2) = -2 - 2a(\cos k_2 - 1) - (V''_{01} + V''_{10}) \quad (56)$$

$$\Delta V'' = V''_{01} - V''_{10} \quad (57)$$

As in the case of the steady state, the integral (55) is differentiated, and evaluated on (one-half) a closed loop

$$\frac{dI(g)}{dg} = \frac{1}{2\pi} \frac{1}{2} \oint_{\Gamma} \frac{dz}{iz} \frac{1}{g(a, k_2) \pm \sqrt{4z^2 + \Delta V''^2}}, \quad (58)$$


When rationalized, the integrand is found to have poles at

$$z_0 = 0 \quad z_{\pm} = \pm \frac{\sqrt{g^2(a, k_2) - \Delta V''^2}}{2}. \quad (59)$$

While z_0 is always enclosed by the unit circle in the complex plane, we need $|z_{\pm}(a, k_2)| < 1$ in order for these poles to contribute to the integral. From the numerics in Fig. 4, it is noted that for weak lattice couplings only the pole z_0

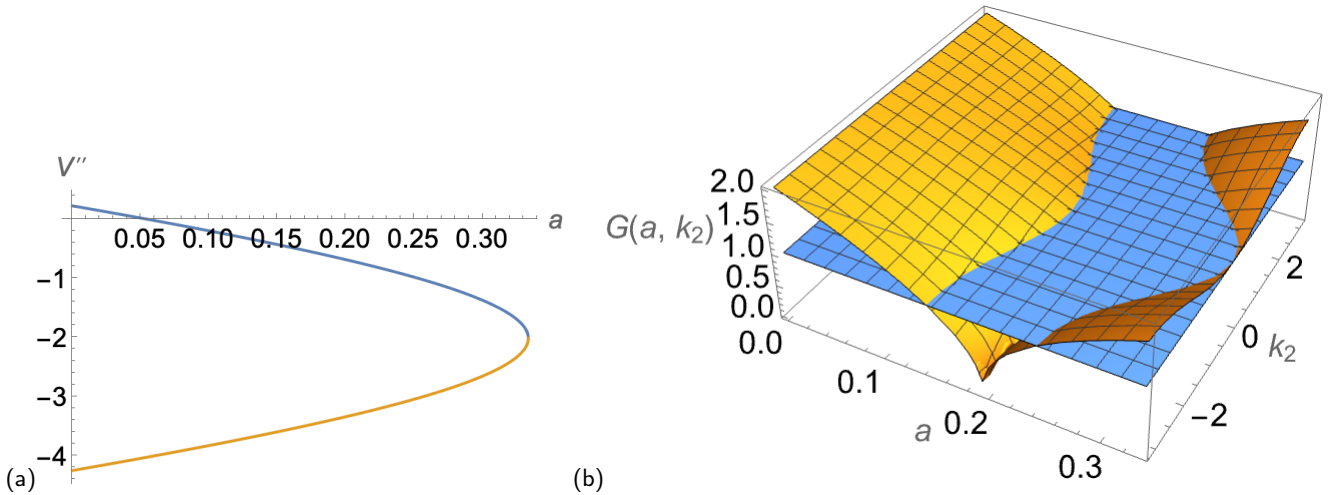


Figure 4: (a) The expressions V''_{01} (blue) and V''_{10} (yellow) vs. coupling a . (b) The range of a and k_2 that make $|z_{\pm}(a, k_2)| < 1$ is determined by the intersection of the function $G(a, k_2) = \sqrt{g^2(a, k_2) - \Delta V''^2}/2$ (in orange, T_2 model) with the plane $z = 1$ (in blue). When $G(a, k_2)$ lies above the plane, only one pole contributes to the contour integral (58), otherwise all three poles in Eq. (59) do, which changes the outcome of the Bravais stability.

contributes to the integral and thus to the Bravais stability of the orbit, whereas in the interval $a \in [0.1835, 0.2404]$ the

contribution comes from all three poles in (59) for all k_2 . In that interval of the coupling strength, the synchronized state (46) is *stable* to perturbations of all spatial frequencies k_2 (Ref. [16]). As a consequence, we should expect this periodic orbit to also be stable under incoherent perturbations, meaning $\lambda = 0$, within the same interval.

In the light of this observation, the evaluation of the double integral (54) is split into the following intervals:

1. $a \in [0, 0.1409]$: there is only the pole $z_0 = 0$ within the unit circle, so that

$$\frac{dI^\pm(g)}{dg} = \frac{1}{2} \frac{1}{g(a, k_2) \pm \Delta V''}, \quad (60)$$

$$I^\pm(g) = \frac{1}{2} \ln |g(a, k_2) \pm \Delta V''| + C_\pm = \frac{1}{2} \ln |(a-1) - V''_\pm - a \cos k_2|, \quad (61)$$

where $V''_+ = V''_{10}$ and $V''_- = V''_{01}$, in the above notation. The additive constant $C_\pm = -\frac{1}{2} \ln 2$ is determined so that

$$\lambda_+(a=0) + \lambda_-(a=0) = I^+(a=0, k_2) + I^-(a=0, k_2) = \frac{1}{2} \ln |T'(\phi_{01})T'(\phi_{10})|, \quad (62)$$

as one would expect in the zero-coupling ($a=0$) case. Then

$$\lambda_\pm = \frac{1}{2\pi} \int_{-\pi}^{\pi} dk_2 \frac{1}{2} \ln |(a-1) - V''_\pm - a \cos k_2| = \frac{1}{2} \ln \frac{a-1 - V''_\pm + \sqrt{(a-1 - V''_\pm)^2 - a^2}}{2}, \quad (63)$$

and $\lambda = \lambda_+ + \lambda_-$, with the outcome is shown in Fig. 5(a) in the blue solid line. A sharp decrease of the instability with the coupling is noted.

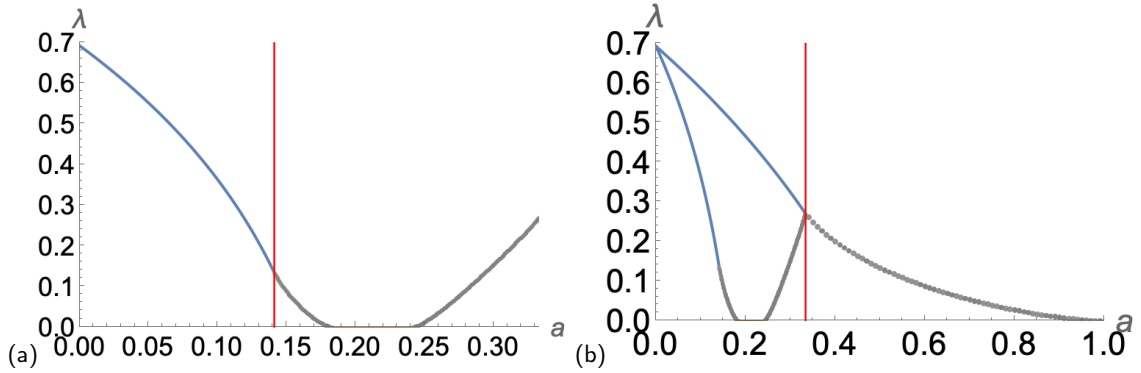


Figure 5: (a) The stability exponent λ versus strength of coupling a for the period-2 synchronized state in the T_2 model. (b) Comparison of λ with the steady synchronized state $\phi = -1/2$ of the same model.

2. $a \in [0.1409, 0.1835]$: the integral in dk_1 may have either one or three poles within the unit circle, depending on the value of k_2 . There are three poles in the interval $k_2 \in [-\pi, -k_2^*] \cup [k_2^*, \pi]$, where k_2^* solves the equation $\frac{\sqrt{g^2(a, k_2) - \Delta V''^2}}{2} = 1$. When $a \simeq 0.1409$, $k_2^* \simeq \pi$ and there is still only the pole $z_0 = 0$ contributing to the integral. As a increases from that value, k_2^* decreases, and the contributions of the poles z_\pm add up to that of z_0 to yield

$$\frac{dI^\pm(g)}{dg} = \frac{1}{2} \frac{1}{g(a, k_2) \pm \Delta V''} - \frac{1}{2} \left(\frac{g(a, k_2)}{g^2(a, k_2) - \Delta V''^2} \mp \frac{g(a, k_2)}{g^2(a, k_2) - \Delta V''^2} \right). \quad (64)$$

When computing λ_+ , the term in parenthesis vanishes, which results in the expression (60), leading to Eq. (63) with a + sign. The other Bloch band gives λ_- by summing up all terms of $\frac{dI^-(g)}{dg}$ in Eq. (64), and integrating

over g . The result is an integral in dk_2 split over the interval $[-\pi, \pi]$, with one pole contributing in $[-k_2^*, k_2^*]$, and three poles in the complement:

$$\lambda_- = \frac{1}{2\pi} \left[\int_{-k_2^*}^{k_2^*} \frac{1}{2} \ln |(a-1) - V_{01}'' - a \cos k_2| dk_2 - 2 \int_{k_2^*}^{\pi} \frac{1}{2} \ln |(a-1) - V_{10}'' - a \cos k_2| dk_2 \right]. \quad (65)$$

Combining with λ_+ [Eq. (63)], one obtains

$$\lambda_+ + \lambda_- = \frac{1}{2\pi} \left[\int_{-k_2^*}^{k_2^*} \frac{1}{2} \ln |(a-1) - V_{01}'' - a \cos k_2| dk_2 + \int_{-k_2^*}^{k_2^*} \frac{1}{2} \ln |(a-1) - V_{10}'' - a \cos k_2| dk_2 \right]. \quad (66)$$

The above integrals are evaluated numerically and the outcome is shown again in Fig. 5 (a) in the dotted gray line that begins at the red vertical line, with the stability further decreasing to vanish at the end of the interval.

3. $a \in [0.1835, 0.2404]$: k_2^* vanishes and therefore the three poles contribute to the contour integrals over the whole $[-\pi, \pi]$ interval. Consequently, the λ_+ and λ_- contributions cancel each other and the Bravais stability to incoherent perturbations is identically zero [just set $k_2^* = 0$ in the integrals of Eq. (66)]. This result is consistent with the finding [16] that this synchronized state becomes stable to perturbations of all space frequencies k_2 in this domain of coupling strengths.
4. $a \in [0.2404, 1/3]$: the configuration of the poles of the contour integral (58) is complementary to the one found for the case $a \in [0.1409, 0.1835]$ [Fig. 4 (b)], therefore the limits of integration of the λ_- contribution to the stability exponent are swapped in the two integrals from Eq. (65):

$$\lambda_- = \frac{1}{2\pi} \left[- \int_{-k_2^*}^{k_2^*} \frac{1}{2} \ln |(a-1) - V_{10}'' - a \cos k_2| dk_2 + 2 \int_{k_2^*}^{\pi} \frac{1}{2} \ln |(a-1) - V_{01}'' - a \cos k_2| dk_2 \right], \quad (67)$$

Combining with λ_+ , one obtains

$$\lambda_+ + \lambda_- = \frac{1}{2\pi} \left[\int_{k_2^*}^{\pi} dk_2 \ln |(a-1) - V_{01}'' - a \cos k_2| + \int_{k_2^*}^{\pi} dk_2 \ln |(a-1) - V_{10}'' - a \cos k_2| \right], \quad (68)$$

exhibiting an unexpected increase in instability in this last interval of a .

For comparison, Fig. 5 (b) features both the behavior of the two Bravais exponents of the steady state $\phi = 1$ and of the period-two orbit. It is noted that the steady state smoothly decreases its instability with the lattice coupling strength, which supports the intuition of collective behavior emerging in tighter lattices. On the contrary, a synchronized state of time period as low as two is long enough to showcase a nontrivial range of instabilities to both coherent and incoherent perturbations. Its Bravais exponent first rapidly drops off to completely vanish at a relatively weak coupling, to then resurge at tighter bindings, before the synchronized state itself disappears altogether (becoming complex valued) at $a = 1/3$.

5. Discussion

Nonlinear field theories with defining equations of the type (1) feature several interesting phenomena, which can efficiently be modeled by means of coupled map lattices [5]. In the framework of spatiotemporal chaos, the search for and characterization of recurrent patterns often proves especially insightful [42, 34, 13]. In particular, understanding the stability of periodic orbits to perturbations is essential for example to separate laminar from turbulent solutions [26], and thus it lies at the core of the dynamical analysis.

In the present work, linear stability analysis has been performed so as to treat space and time on equal grounds. This approach is made possible by the spatiotemporal orbit Jacobian operator, in both phase-space and reciprocal lattice, where frequencies replace space and time to identify perturbations. Once the type of stability of periodic orbits to periodic (coherent) perturbations of a certain space or time frequency is determined, the stability to aperiodic (incoherent) perturbations is also computed by summing all the eigenvalues of the orbit Jacobian operator over all frequencies.

In the specific model of coupled Chebyshev maps, changes of stability may occur as a function of the coupling strength, and, as shown in this venue, the shortest synchronized states of this lattice model already showcase a number of different scenarios. Synchronized states are the simplest periodic orbits, which allow for an almost fully analytic treatment of the problem of linear stability to both coherent and incoherent perturbations. Here, doing the calculations mostly by hand enables us to unravel the connections between the stability type of steady states or time period-2 orbits to perturbations of definite frequencies, and that to general, aperiodic perturbations, thanks to complex analysis (contour integration). Regarding the ('Bravais') stability to incoherent perturbations, the findings that stem from the present analysis are expected and intuitive for the synchronized steady states: stronger coupling enhances collective motion and thus reduces instability from the anti-integrable limit. Less obvious is the behavior of the time period-2 synchronized state, which turns from unstable to stable and then back to unstable as the coupling strength is increased, before becoming complex valued and thus disappearing from the real lattice space. While the previous observations were made in [16] following the temporal analysis of perturbations of definite space frequencies, here they are confirmed in the full spatiotemporal picture (from the computation of the orbit Jacobian operator), and extended to incoherent perturbations.

Based on the present results, it is legitimate to expect a richer landscape of bifurcations when more complex, non-synchronized recurrent spatiotemporal patterns are considered. A hint already is given to us by both the phase diagram of the time period-2 synchronized state discussed above, and by its interaction with a steady state, portrayed in Fig. 5(b). While the quantities of interest and the salient formulae (such as the double integral (29) for the Bravais stability) would be unchanged, more serious computational hurdles would certainly call for numerics in their evaluations, instead of the elegant formal analysis performed here.

Linear stability analysis of periodic states, and more in general of recurrent patterns, is instrumental for the computation of partition sums in deterministic chaotic field theories [30, 33, 15]. There, the Bravais stability exponent of each orbit constitutes the weight of the corresponding term in the partition functional, that generates expectation values for all observables of interest in the theory. For example, in chaotic classical field theories such as Kuramoto-Sivashinskii [12], Yang-Mills, or Navier-Stokes [14], global averages such as Lyapunov exponents or correlation functions can be evaluated by means of spatiotemporally periodic patterns. In Beck's theory [4] of chaotic strings, a number of parameters of the standard model of particle physics were computed by means of averages of interactions and self-energies with a precision of four digits with direct numerical simulations, while temporal periodic orbit theory could demonstratively attain 13 significant figures for some of the same quantities on a two-site lattice [17]. Most recently, spatiotemporal chaos shows up in lattice QED [29], where stochastic quantization is applied to evaluate the anomalous magnetic moment of the electron by numerical averaging [28]. Recurrent patterns may prove effective and insightful in this class of problems, as well.

With that perspective, this work is but the beginning of a systematic study of the spatiotemporal stability properties of periodic states in a dissipative, or non phase-space volume preserving, class of systems.

6. Acknowledgements

The author thanks P. Cvitanović for valuable discussions. This work has been supported by JSPS KAKENHI Grant No. 25K07154 (PI: A. Shudo).

A. Appendix: Evaluation of the Bravais stability exponent for a steady state

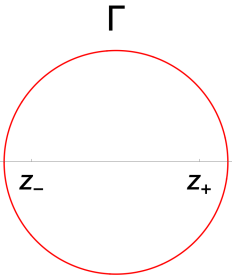
Let us evaluate the integral (39) with the residue theorem, dropping the absolute value in the argument of the logarithm:

$$\lambda = \frac{1}{2\pi} \int_{-\pi}^{\pi} dk_2 \ln [(1-a)T'_N(\phi_p) + a \cos k_2] . \quad (69)$$

Now call $\xi(a) = (1-a)T'_N(\phi_p)$, and evaluate the quantity

$$\frac{d\lambda}{d\xi} = \frac{1}{2\pi} \int_{-\pi}^{\pi} \frac{dk_2}{\xi(a) + a \cos k_2} . \quad (70)$$

The previous is rewritten as the contour integral (let $z = e^{ik_2}$)

$$\frac{1}{2\pi} \oint_{\Gamma} \frac{dz}{iz} \frac{2}{2\xi(a) + a(z + z^{-1})}$$


(71)

The integrand has two poles, $z_{\pm} = \frac{-\xi(a) \pm \sqrt{\xi^2(a) - a^2}}{a}$, both real-valued for $\xi^2(a) - a^2 > 0$, or, equivalently,

$$a < \frac{|T'_N(\phi_p)|}{1 + |T'_N(\phi_p)|}. \quad (72)$$

One can now evaluate (71) using the residue theorem:

$$\frac{d\lambda}{d\xi} = \frac{1}{2\pi} \oint \frac{dz}{2\xi(a)z + \frac{a}{2}z^2 + \frac{a}{2}} = \frac{1}{2\pi} \oint \frac{dz}{\frac{a}{2}(z - z_-)(z - z_+)}. \quad (73)$$

How many poles lie within the unit circle? Requiring $|z_{\pm}| < 1$, it turns out that there is only one pole (either z_+ or z_-) within the unit circle in the interval of a verifying inequality (72). Then,

$$\frac{d\lambda}{d\xi} = \pm \frac{1}{\frac{a}{2}(z_- - z_+)} = \pm \frac{1}{\sqrt{\xi^2(a) - a^2}}. \quad (74)$$

Integrating Eq. (74) with respect to ξ and imposing the boundary condition $\lambda(a = 0) = \ln |T'_N(\phi_p)|$ (uncoupled lattice), we retrieve the result (40):

$$\lambda = \ln \frac{(1 - a)|T'_N(\phi_p)| + \sqrt{(1 - a)^2 T_N'^2(\phi_p) - a^2}}{2}. \quad (40)$$

Importantly, λ is a real number in the whole interval of validity of the previous expression, that is for

$$a < \frac{|T'_N(\phi_p)| - 1}{|T'_N(\phi_p)| + 1}, \quad (75)$$

marked by the red vertical line in Fig. 3. The previous condition comes from Eq. (35) for the integral in the time-frequency k_1 to be nonzero, in which one sets $\cos k_2 = \pm 1$, depending on the sign of $T'_N(\phi_p)$.

Beyond that value of a , the limits of integration reduce to $-k_2^*$, k_2^* defined by Eq. (43):

$$\lambda = \frac{1}{2\pi} \int_{-k_2^*}^{k_2^*} dk_2 \ln[(1 - a)T'_N(\phi_p) + a \cos k_2]. \quad (76)$$

In the main text, the integral of the $\ln[...]$ was computed numerically, since we are interested in the real part of the stability exponent λ . However, one may wonder if and for what couplings the argument of the log turns negative in Eq. (76), and consequently λ acquires an imaginary part. From the previous expression, we may infer that the argument of the logarithm is positive for

$$a < \frac{|T'_N(\phi_p)|}{|T'_N(\phi_p)| + 1}, \quad (77)$$

since $\cos k_2 \in [\cos k_2^*, 1]$, depending on k_2^* , so that Eq. (77) yields the smallest a that produces a complex-valued λ . Recalling Eq. (75), we may conclude that for

$$\frac{|T'_N(\phi_p)| - 1}{|T'_N(\phi_p)| + 1} < a < \frac{|T'_N(\phi_p)|}{|T'_N(\phi_p)| + 1}, \quad (78)$$

the Bravais stability exponent is real valued. The apparent inflection point (Fig. 3) observed for values of the coupling strength across condition (75) is then due to the functional change of $\lambda(a)$: from equation (69) with fixed limits of integration, to Eq. (76), where the a -dependence is the same in the integrand, but now it also appears in the the limits of integration, with k_2^* a function of a through Eq. (43).

Let us get as close as possible to a primitive for the integral (76): leverage the trigonometric identity $\cos k_2 = 1 - 2 \sin^2 \frac{k_2}{2}$, and operate the substitution $P^2 = 4 \sin^2 \frac{k_2}{2}$. That way, the integral (76) is rewritten as

$$\lambda = \frac{\ln a/2}{2\pi} \int_{-P^*}^{P^*} dP \frac{\ln(\mu^2 - P^2)}{\sqrt{1 - P^2/4}}, \quad (79)$$

where $\mu^2 = 2 \frac{(1-a)T'_N(\phi_p)+a}{a}$. Splitting $\mu^2 - P^2 = (\mu - P)(\mu + P)$, integrating by parts, and regrouping, produces the outcome

$$\lambda = \frac{\ln a/2}{2\pi} \left[\arcsin P \ln(\mu^2 - 4P^2) \Big|_{-P^*/2}^{P^*/2} + 2 \int_{-P^*/2}^{P^*/2} dP \frac{P \arcsin P}{\mu^2 - 4P^2} \right], \quad (80)$$

where the latter term may be written in terms of polylogarithmic functions. Looking at the integrand of Eq. (79) and recalling the definition of μ , we once again obtain the condition (77) for the logarithm and thus the Bravais exponent to be real valued. For stronger coupling, the stability exponent becomes complex valued, and thus perturbations drive the field away from the synchronized state ϕ_p but this time in an oscillatory fashion.

References

- [1] Alderson, W., Dubertrand, R., Shudo, A., 2025. Classical transport in a maximally chaotic chain. *J. Phys. A* 58, 165201. doi:10.1088/1751-8121/adc217.
- [2] Amritkar, R.E., Gade, P.M., Gangal, A.D., Nandkumaran, V.M., 1991. Stability of periodic orbits of coupled-map lattices. *Phys. Rev. A* 44, R3407–R3410. doi:10.1103/PhysRevA.44.R3407.
- [3] Barkley, D., 2011. Simplifying the complexity of pipe flow. *Phys. Rev. E* 84, 016309. doi:10.1103/PhysRevE.84.016309.
- [4] Beck, C., 1995. Chaotic quantization of field theories. *Nonlinearity* 8, 423–441. doi:10.1088/0951-7715/8/3/008.
- [5] Beck, C., 1997. Coupled map lattices simulating hydrodynamical turbulence. *Physica D* 103, 528–536. doi:10.1016/s0167-2789(96)00283-7.
- [6] Bohr, T., Jensen, M.H., Paladin, G., Vulpiani, A., 1998. *Dynamical Systems Approach to Turbulence*. Cambridge Univ. Press, Cambridge. doi:10.1017/cbo9780511599972.
- [7] Bountis, T., Helleman, R.H.G., 1981. On the stability of periodic orbits of two-dimensional mappings. *J. Math. Phys.* 22, 1867–1877. doi:10.1063/1.525159.
- [8] Bunimovich, L.A., Lambert, A., Lima, R., 1990. The emergence of coherent structures in coupled map lattices. *J. Stat. Phys.* 61, 253–262. doi:10.1007/BF01013964.
- [9] Bunimovich, L.A., Sinai, Y.G., 1988. Spacetime chaos in coupled map lattices. *Nonlinearity* 1, 491. doi:10.1088/0951-7715/1/4/001.
- [10] Chantry, M., Tuckerman, L.S., Barkley, D., 2017. Universal continuous transition to turbulence in a planar shear flow. *J. Fluid Mech.* 824, R1. doi:10.1017/jfm.2017.405.
- [11] Chazottes, J.R., Fernandez, B. (Eds.), 2005. *Dynamics of Coupled Map Lattices and of Related Spatially Extended Systems*. Springer, Berlin.
- [12] Christiansen, F., Cvitanović, P., Putkaradze, V., 1997. Spatiotemporal chaos in terms of unstable recurrent patterns. *Nonlinearity* 10, 55–70. doi:10.1088/0951-7715/10/1/004.
- [13] Crowley, C.J., Pughe-Sanford, J.L., Toler, W., Krygier, M.C., Grigoriev, R.O., Schatz, M.F., 2022. Turbulence tracks recurrent solutions. *Proc. Natl. Acad. Sci.* 119, 120665119. doi:10.1073/pnas.2120665119.
- [14] Cvitanović, P., 2000. Chaotic Field Theory: A sketch. *Physica A* 288, 61–80. doi:10.1016/S0378-4371(00)00415-5.
- [15] Cvitanović, P., Liang, H., 2025. A chaotic lattice field theory in two dimensions. URL: <https://arxiv.org/abs/2503.22972>.
- [16] Dettmann, C.P., 2002. Stable synchronised states of coupled Tchebyscheff maps. *Physica D* 172, 88–102. doi:10.1016/s0167-2789(02)00624-3.
- [17] Dettmann, C.P., Lippolis, D., 2005. Periodic orbit theory of two coupled Tchebyscheff maps. *Chaos Solit. Fract.* 23, 43–54. doi:10.1016/j.chaos.2004.04.017.

- [18] Frisch, U., Hasslacher, B., Pomeau, Y., 1986. Lattice-gas automata for the navier-stokes equation. *Phys. Rev. Lett.* 56, 1505–1508. doi:10.1103/physrevlett.56.1505.
- [19] Gade, P.M., Amritkar, R.E., 1993. Spatially periodic orbits in coupled-map lattices. *Phys. Rev. E* 47, 143–154. doi:10.1103/PhysRevE.47.143.
- [20] Gielis, G., MacKay, R.S., 2000. Coupled map lattices with phase transition. *Nonlinearity* 13, 867–888. doi:10.1088/0951-7715/13/3/320.
- [21] Hagerstrom, A.M., Murphy, T.E., Roy, R., Hövel, P., Omelchenko, I., Schöll, E., 2012. Experimental observation of chimeras in coupled-map lattices. *Nature Physics* 8, 658–661. doi:10.1038/nphys2372.
- [22] Isola, S., Politi, A., Ruffo, S., Torcini, A., 1990. Lyapunov spectra of coupled map lattices. *Phys. Lett. A* 143, 365–368. doi:10.1016/0375-9601(90)90373-V.
- [23] Jiotsa, A.K., Politi, A., Torcini, A., 2013. Convective Lyapunov spectra. *J. Phys. A* 46, 254013. doi:10.1088/1751-8113/46/25/254013.
- [24] Kaneko, K., 1983. Transition from torus to chaos accompanied by frequency lockings with symmetry breaking: In connection with the coupled-logistic map. *Prog. Theor. Phys.* 69, 1427–1442. doi:10.1143/PTP.69.1427.
- [25] Kaneko, K., 1984. Period-doubling of kink-antikink patterns, quasiperiodicity in antiferro-like structures and spatial intermittency in coupled logistic lattice: Towards a prelude of a “field theory of chaos”. *Prog. Theor. Phys.* 72, 480–486. doi:10.1143/PTP.72.480.
- [26] Kawahara, G., Kida, S., Nagata, M., 2005. Unstable periodic motion in plane Couette system: The skeleton of turbulence, in: Meier, G.E.A., Sreenivasan, K.R., Heinemann, H.J. (Eds.), *One Hundred Years of Boundary Layer Research*, Springer, Dordrecht.
- [27] Killinback, T., Loftus, G., Sundaram, B., 2013. Competitively coupled maps and spatial pattern formation. *Phys. Rev. E* 87, 022902. doi:10.1103/PhysRevE.87.022902.
- [28] Kitano, R., 2024. QED five-loop on the lattice. *Prog. Theor. Exp. Phys.* 2025, Prog. Theor. Exp. Phys. doi:10.1093/ptep/ptae194.
- [29] Kitano, R., Takaura, H., Hashimoto, S., 2021. Stochastic computation of $g-2$ in QED. *J. High Energy Phys.* 2021, 199. doi:10.1007/jhep05(2021)119.
- [30] Lan, Y., Cvitanović, P., 2008. Unstable recurrent patterns in Kuramoto-Sivashinsky dynamics. *Phys. Rev. E* 78, 026208. doi:10.1103/PhysRevE.78.026208.
- [31] Lei, X., Yan, Z., Zhao, H., Gao, J., Lan, Y., Xiao, J., 2026. Symmetry enhanced prediction of spatio-temporal chaotic system with reservoir computing. *Chaos Solit. Fract.* 202, 117634. doi:10.1016/j.chaos.2025.117634.
- [32] Lepri, S., Politi, A., Torcini, A., 1996. Chronotopic Lyapunov analysis. I. A detailed characterization of 1D systems. *J. Stat. Phys.* 82, 1429–1452. doi:10.1007/BF02183390.
- [33] Liang, H., Cvitanović, P., 2022. A chaotic lattice field theory in one dimension. *J. Phys. A* 55, 304002. doi:10.1088/1751-8121/ac76f8.
- [34] Lucas, D., Kerswell, R.R., 2015. Recurrent flow analysis in spatiotemporally chaotic 2-dimensional Kolmogorov flow. *Phys. Fluids* 27, 518–554. doi:10.1063/1.4917279.
- [35] Nozawa, H., 1992. A neural network model as a globally coupled map and applications based on chaos. *Chaos* 2, 377. doi:10.1063/1.165880.
- [36] Parisi, G., Wu, Y.S., 1981. Perturbation-theory without gauge fixing. *Scientia Sinica* 24, 483–496. doi:10.15161/oar.it/1447948233.36.
- [37] Pazó, D., Szendro, I.G., López, J.M., Rodríguez, M.A., 2008. Structure of characteristic Lyapunov vectors in spatiotemporal chaos. *Phys. Rev. E* 78, 016209. doi:10.1103/PhysRevE.78.016209.
- [38] Pecora, L.M., Carroll, T.L., 1990. Synchronization in chaotic systems. *Phys. Rev. Lett.* 64, 821. doi:10.1103/PhysRevLett.64.821.
- [39] Pikovsky, A.S., 1989. Spatial development of chaos in nonlinear media. *Phys. Lett. A* 137, 121–127. doi:10.1016/0375-9601(89)90096-0.
- [40] de San Roman, F.S., Boccaletti, S., Maza, D., Mancini, H., 1998. Weak synchronization of chaotic coupled map lattices. *Phys. Rev. Lett.* 81, 3639. doi:10.1103/PhysRevLett.81.3639.
- [41] Tenny, R., Tsmiring, L.S., Larson, L., Abarbanel, H.D.I., 2003. Using distributed nonlinear dynamics for public key encryption. *Phys. Rev. Lett.* 90, 047903. doi:10.1103/PhysRevLett.90.047903.
- [42] Viswanath, D., 2007. Recurrent motions within plane Couette turbulence. *J. Fluid Mech.* 580, 339–358. doi:10.1017/S0022112007005459.